International Journal of Intelligent Information and Management Science
ISSN: 2307-0692, Volume 6, Issue 5, October, 2017

Design and Control of A New Bearingless Motor for Flywheel Energy Storage

Fan Yang
School of Electrical and Information Engineering, Jiangsu University, Zhenjiang, China

Abstract: Flywheel energy storage is a new energy storage technology. The existing technology is mainly based on ordinary high-speed motor as the main driving force lead to flywheel energy storage system is inefficient and can't reach the ideal energy conversion efficiency. The new type of 12 slot 8-pole high speed motor is designed based on the structure of a new flywheel energy storage device. It is added suspension winding to the outer rotor brushless DC motor to make it a bearingless motor. Firstly, the structure and size of the motor are described in detail. Secondly, the principle of the motor is introduced in detail and the mathematical model of the motor is derived. Thirdly, the finite element tool is used to simulate the design of the motor. Finally, The simulation system is built using the obtained mathematical model. The simulation of two different states of electric motor and electric generator is carried out. The experimental results show that the parameters of the motor meet the design objectives. It can be used in flywheel energy storage structure and make it more efficient.

Keywords: Flywheel energy storage; Bearingless; Brushless DC motor

1. Introduction

The bearingless Brushless DC Motor can not only rotate but also levitate at the same time via integrating the magnetic suspension winding into the stator of the motor. Moreover, it provides a new approach to solving the problem of brushless DC motor's noise and vibration and has potential application in the area of flywheel energy storage.

Relative to the bearingless asynchronous motor, bearingless permanent magnet synchronous motor and bearingless switched reluctance motor, bearingless brushless DC motor started late for nearly ten years. However, thanks to the growth of high-performance motor demand and a series of advantages of bearingless brushless DC motor, in recent years domestic and foreign scholars have carried out research on bearingless brushless DC motor and achieved a series of results.

The initial design of the bearingless brushless DC motor is based on the general brushless DC motor to add a set of suspension winding to produce suspension force. After the scholars have proposed a non-bearing brushless DC motor and a single winding non-bearing brushless DC motor, but the study of the motor size is small, does not apply to flywheel energy storage device. And the single winding motor, although the motor body to simplify the structure, but the control of the motor a lot of complex, high-speed rotation in the motor when the difficulty of control increased a lot. Later, some scholars have deduced the mathematical model of the suspension force of the bearingless brushless DC motor according to the magnetic circuit method, and verified the mathematical model with the finite element software. But only for the inner rotor double winding bearingless brushless DC motor.

According to the above, in order to cope with the magnetic bearing operation in the flywheel energy storage device, this paper uses 12-slot 8-pole out-rotor bearingless brushless DC motor. The motor axial length is relatively short that can make the flywheel energy storage device structure more concise. And the flywheel energy storage device in the motor needs to work in the electric and power generation two states, select the double winding motor easier to control, in the power generation state can also control the levitation force. Through the control model simulation, you can see the motor can be applied to flywheel energy storage device.

2. Structure of a Motor

Figure1 shows the cross section of the proposed ORBBDM. The stator adopts the salient pole structure. The torque winding and the suspension winding are wound on the stator salient pole in a concentrated winding manner. Torque winding consists of U, V, W three-phase winding, each phase winding consists of four coils, a total of 12. Among them, U1, U2, U3 and U4 windings form U-phase windings in series. V1, V2, V3 and V4 windings form a V-phase winding in series. W1, W2, W3 and W4 windings form W-phase windings in series. Each coil is wound around a stator tooth and is distributed in the clockwise direction in the order U1→V1→W1→U2→V2→W2→U3→V3→W3→U4→V4→W4.

Suspension winding consists of six sets of windings, each pair of relative stator teeth on the coil in series to form a suspension force winding, a1, a2, b1, b2, c1, c2 a total of six sets. Since the mutual inductance between the concentrated windings is very small, and the torque winding and the suspension force winding of the coals do not always energize at the same time, the decoupling control between the torque and the suspension force can be realized.

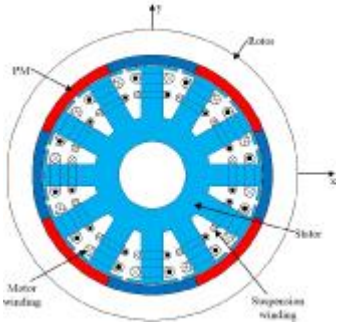

Figure 1. The Structure of ORBBDM

3. Mathematical Model of Suspension Force

Based on the above analysis, the principle of the radial suspension force of the 12 groove and the 8 pole structure is studied. A case study is carried out to analyze the single degree of freedom of the rotor along the X axis when the rotor winding of A1 is used to control the rotor suspension. The motor structure of the suspension force winding A1 is shown in figure 2. Winding A1 consists of series connected windings a11 and a12. The thickness of permanent magnet is hm. Stator inner diameter is r. Stator outer diameter is R. Rotor shaft length is l. The average air gap length is δ. The turns of windings a11 and a12 are N. The pole arc angle is θr. In order to ignore the influence of rotor gravity, motor vertical placement. Therefore, the resultant force of the rotor in the equilibrium position is 0, that is, the suspension force winding current is about 0. At this time, the forward displacement of the rotor along the X axis is x. The direction of the current in the winding is shown in Figure 3.

There are the same amplitude and opposite direction in the suspension force winding a11 and a12. So the induced current is 0. To facilitate the derivation of the formula, the following assumptions are made: (1) the mutual inductance between the core reluctance, magnetic flux leakage, edge flux and concentrated winding is neglected. (2) Core free saturation. (3) The recovery magnetic permeability of the permanent magnet is 1, and the demagnetization curve coincides with the recovery line. (4) The rotor yoke stator inner circle and outer circle as the boundary condition. According to the similarity of the magnetic circuit of the suspension force a11 and the a12, the equivalent magnetic circuit of the x axis is shown in Figure 3. The upper and lower sides correspond to the equivalent magnetic path of the right portion of the suspensional force winding a11 and the left portion of the suspension force winding a12, respectively.

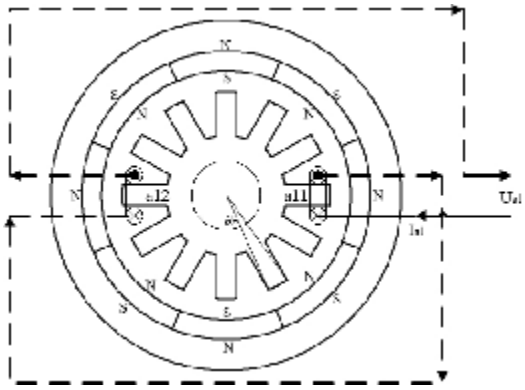

Figure 2.Principle of Suspension Force Generation

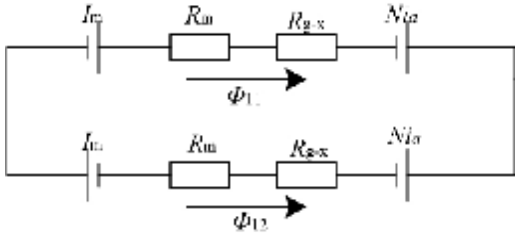

Figure 3.Equivalent Magnetic Circuit

Resultant force of rotor eccentricity:

$$\boldsymbol{F} \approx \frac{\boldsymbol{N}^2\mu_0\boldsymbol{S}(\frac{\boldsymbol{I}_m}{\boldsymbol{N}}+\boldsymbol{i}_a)^2}{2(\boldsymbol{h}_m+\delta)}[\frac{1}{\boldsymbol{h}_m+\delta}+\frac{2\boldsymbol{x}}{(\boldsymbol{h}_m+\delta)^2}] \qquad (1)$$

Regardless of the role of the axial force of the bearingless brushless DC motor, the rotor is mainly subjected to two forces, namely the tangential force and the radial force. Tangential force control rotor rotation. Radial force control rotor suspension. Radial force is divided into two kinds. One is due to the magnetic force between the permanent magnet and the stator core on the rotor. When the rotor is not eccentric, the magnetic force of the rotor is zero due to the symmetrical distribution of the stator core along the circumference. When the rotor is eccentric, the magnetic force is no longer is 0, that is, produced along the eccentricity that the air gap length of the direction of the unbalanced magnetic tension. The second type is due to the rotor eccentricity, the need to pass in the suspension force winding current, this part of the current generated by the electromagnetic force to overcome the rotor by the unbalanced magnetic tension, so that the resultant force of the rotor is always toward the center of the stator. So the unbalanced magnetic tension and the magnetic force generated by the cantilever windings are always in

pairs in the opposite direction, and the two interact with each other to stabilize the rotor.

Unbalanced magnetic tension is generated by the interaction between the permanent magnet and the stator core, and therefore only with the equivalent current of the permanent magnet, that is, ia = 0 in equation (2). Due to the uniform distribution of the stator teeth and the rotor permanent magnet along the respective circumferential surfaces, it is considered that the magnetic force of all the stator teeth on the rotor deviates from the center of the stator, that is, the first term of the polynomial in equation (2) is zero, so only the polynomial The second item can be. the six pairs of teeth on both sides of the y-axis produce unbalanced magnetic tension, and the total unbalanced magnetic tension is

$$\begin{aligned} F_x &= \frac{2B_r^2 h_m^2 S}{\mu_0 (h_m + \delta)^3}(1 + 2\cos^2 30^\circ + 2\cos^2 60^\circ)x \\ &= \frac{6B_r^2 h_m^2 S}{\mu_0 (h_m + \delta)^3} x \end{aligned} \tag{2}$$

Ignoring the second term of equation (2), the electromagnetic force of the rotor is caused by the interaction between the magnetic field of the suspension force and the magnetic field of the permanent magnet, and therefore the sum of the suspension force winding current and the equivalent current of the permanent magnet (ia + Im / N). So the suspension force winding a1 on the rotor of the electromagnetic force is

$$F_{a1} = F_{a11} - F_{a12} = \frac{2SB_r h_m N}{(h_m + \delta)^2} i_a \tag{3}$$

According to the above analysis of the unbalanced magnetic tension and the electromagnetic force generated by the cantilever windings, it can be seen that the radial force of the rotor along the x-axis is

$$F_{sa1} = F_{a1} + F_x = \frac{2SB_r l_m N}{(l_m + \delta)^2} i_a + \frac{6B_r^2 l_m^2 S}{\mu_0 (l_m + \delta)^3} x \tag{4}$$

Can be written as

$$F_{sa1} = k_i i_a + k_x x \tag{5}$$

Where: ki is the current stiffness coefficient; kx is the displacement stiffness coefficient, the concrete expression is (12) and (13).

$$k_i = \frac{2SB_r l_m N}{(l_m + \delta)^2} \tag{6}$$

$$k_x = \frac{6B_r^2 l_m^2 S}{\mu_0 (l_m + \delta)^3} \tag{7}$$

4. Magnetic Suspension Control Method

Figure 4 shows the control system configuration of the proposed bearingless brushless dc motor. In the control system, the motor controller is quite same as that of the conventional brushless dc motors. Hence, the magnetic suspension controller is explained in details below.

Figure 4 shows the configuration of the control system. In the motor controller, the rotor angular position is detected every 30 mechanical degrees by Hall sensors. For the current command IM* and the detected angular position , the current commands iU*, iV* and iW* in the U-, V- and W-phase motor windings are determined. The motor winding currents iU, iV and iW follow the current commands.

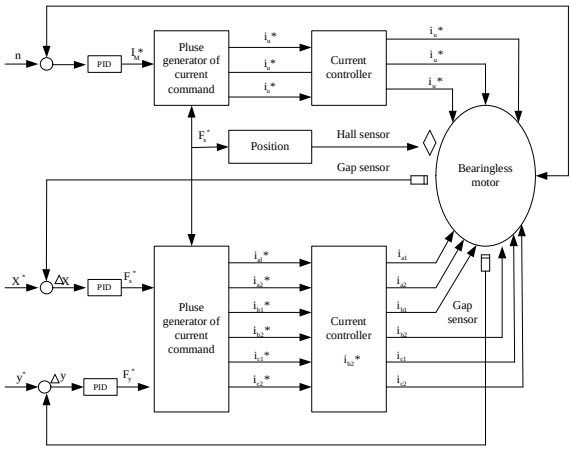

Figure 4.Control System Configuration

A description of how the suspension winding sets are selected to stably support the rotor shaft is provided below. The radial position of the rotor is detected along two perpendicular axes (x and y) by the gap sensors. The difference between the detected rotor radial position and the position command is amplified by a Proportional-Integral- Derivative (PID) Controller on the x and y axes and, as a result, the suspension force commands Fx* and Fy* are determined. When the rotor angular position is within the ranges of 0 to 15 mechanical degrees and 45 to 60 mechanical degrees, the suspension windings b1 and b2 are excited. The suspension force commands Fx* and Fy* are transformed into the Fb1* and Fb2* in the b1- and b2-axes, where the directions of MMFs of the suspension windings b1 and b2 are defined as. The current commands ib1* and ib2* for the suspension windings b1 and b2 are determined to be proportional to the Fb1* and Fb2* so that

$$\begin{bmatrix} i_{b1}^* \\ i_{b2}^* \end{bmatrix} = K \begin{bmatrix} F_{b1}^* \\ F_{b2}^* \end{bmatrix} = K \begin{bmatrix} \cos 120^\circ & \sin 120^\circ \\ -\sin 120^\circ & \cos 120^\circ \end{bmatrix} \begin{bmatrix} F_x^* \\ F_y^* \end{bmatrix} \tag{8}$$

where K is a current constant. Note that the b1- and b2-axes are rotated by 120 degrees in the x- and y-axes.

For the angular position ranges of 15 to 30 degrees and 60 to 75 degrees, the suspension windings a1 and a2 are excited. The suspension force commands Fx* and Fy* are transformed into the Fa1* and Fa2* in the a1- and a2-axes. The current commands ia1* and ia2* in the suspension windings a1 and a2 are similarly determined where

$$\begin{bmatrix} i_{a1}^* \\ i_{a2}^* \end{bmatrix} = K \begin{bmatrix} F_{a1}^* \\ F_{a2}^* \end{bmatrix} = K \begin{bmatrix} F_x^* \\ F_y^* \end{bmatrix} \tag{9}$$

Note that the a1 and a2 axes correspond to the x- and y-axes.

Finally, for the angular position ranges of 30 to 45 degrees and 75 to 90 degrees, the suspension windings c1 and c2 are excited. The suspension force commands Fx* and Fy* are transformed into the Fc1* and Fc2* in the c1- and c2-axes. The current commands ic1* and ic2* are determined where

$$\begin{bmatrix} i_{c1}^* \\ i_{c2}^* \end{bmatrix} = K \begin{bmatrix} F_{c1}^* \\ F_{c2}^* \end{bmatrix} = K \begin{bmatrix} \cos 240^\circ & \sin 240^\circ \\ -\sin 240^\circ & \cos 240^\circ \end{bmatrix} \begin{bmatrix} F_x^* \\ F_y^* \end{bmatrix} \quad (10)$$

where the c1 and c2 axes are rotated by 240 mechanical degrees from the x- and y-axes. According to (1)-(3) above, the rotor shaft is stably suspended without the mechanical contact.

Figure 5 shows a set of example waveforms for the current commands of the suspension windings when a suspension force is required along the x axis. The suspension winding currents are square waveforms with the same frequency as the motor winding current. The current commands ia2* for the suspension winding a2 is zero when a suspension force is generated along the x axis only.

It can be observed that even though motor and suspension windings may wound around the same stator tooth, they are not excited at the same time. For example, during a rotor angular position of between 0 and 15 degrees, the U-phase motor winding is excited; however, the suspension windings a1 and a2, which is wound on the same stator teeth as the Uphase motor winding, are not excited. This means that the coupling and mutual interference between the motor and suspension windings is very small. Hence, by use of the proposed magnetic suspension control method, the motor can be stably suspended without the mechanical contact.

An EMF is induced by the PM flux into each suspension winding; however, because of the series connection of opposite coils, the net sum of these EMFs is zero since they are linked by an equal and opposite magnet flux. Therefore the PM flux does not influence the current commands in the suspension windings.

5. Experimental Results

Figure 6 Schematic diagram of the motor. The motor is an outer rotor structure with four air gap sensors on the outside to detect the rotor position. Two gap sensors are equipped along two perpendicular radial axes, respectively.

Fig. 8 shows motor torque current stable waveform. This value to achieve the set target of motor power.

Fig. 9 shows motor speed waveform. The simulation of the motor speed is set to 5000 rpm. The simulation shows that the target is well established.

Fig. 10 shows the motor rotor displacement waveform. The rotor is always moving around the center. The results show that this control method can be used to control the motor suspension.

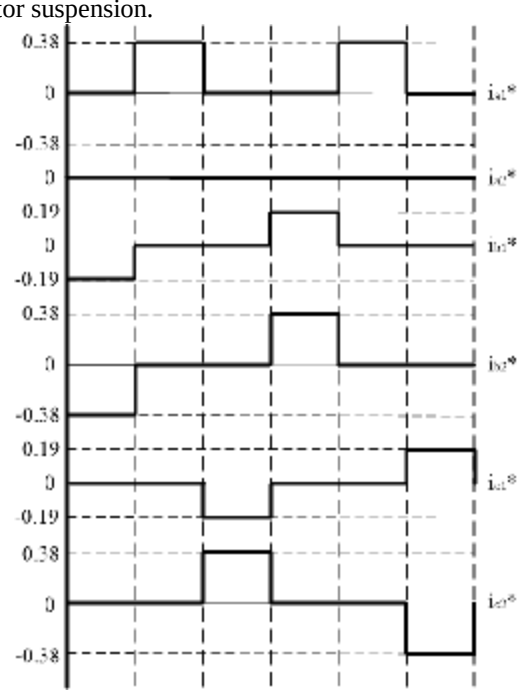

Figure 5.Waveform of Suspension Winding Current Commands

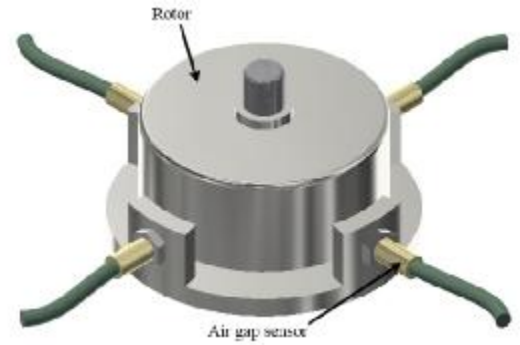

Figure 6. Schematic Siagram of Motor Model

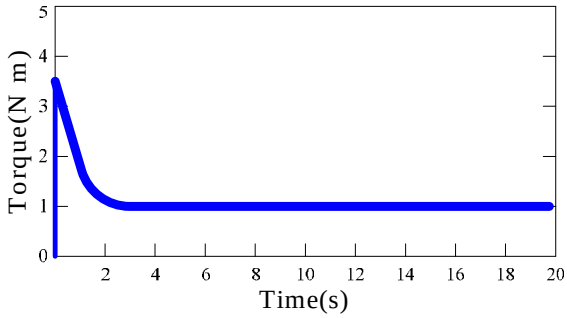

Figure 7. Shows the Motor Torque Waveform. Torque Stability After the Value of 1N·m. This Value Meets the Design Requirements of the Motor.

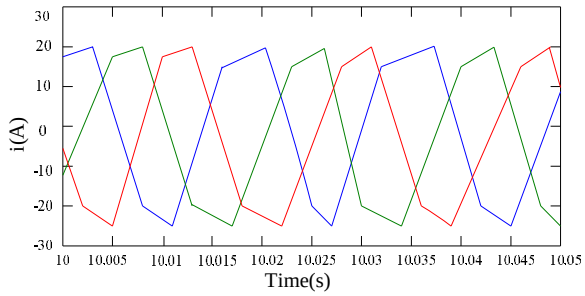

Figure 8. Current Stable Waveform

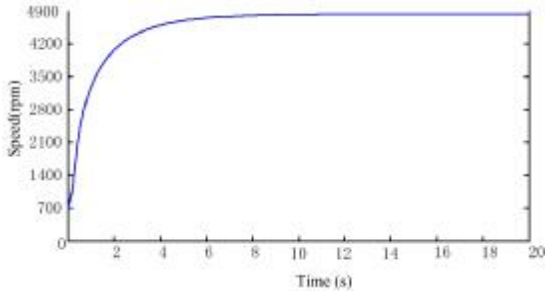

Figure 9. Speed Waveform

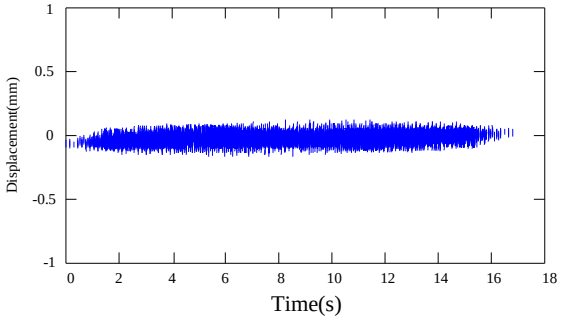

Figure 10. Speed Waveform

6. Conclusion

The bearingless brushless DC motor is applied to the flywheel energy storage in the article. The motor generally works above 5000 rpm. The motor increases the suspension winding to produce suspension force in order to solve the problem of high mechanical loss when the speed is high. The use of external rotor structure makes the flywheel energy storage device structure simplified. The mathematical model of the motor awakened the derivation. Through the finite element simulation can be seen that the motor can produce a stable suspension force and does not affect the performance of the original motor. The motor meets the design goals and meets the requirements of the motor in the flywheel energy storage device. The prototype is further validated for the design of the motor in future. And further improve the motor speed to reach 20,000 rpm.

References

[1] Ooshima M., Takeuchi C., "Magnetic suspension performance of a bearingless brushless DC motor for small liquid pumps," IEEE Tran. Industry Applications, Vol. 47-1, pp. 72-78, 2011.

[2] Zhang, Weiyu. "Key Technologies and Development Status of Flywheel Energy Storage System," Transactions of China Electrotechnical Society, vol.26-7, pp. 141-146, 2011.

[3] W. Amrhein, S. Silber, and K. Nenninger, "Suspension forces in bearingless permanent magnet motors," IEEE Trans. Magnetics, vol. 35, no. 5, pp. 4052–4054, Sep. 1999.

[4] Chiba A., Asama J. "Influence of rotor skew in induction type bearingless motor," IEEE Trans. Magn, Vol. 48-11, pp. 4646-4649, 2012.

[5] Hak-In Lee, Seong-yeol Yoo, Noh M. D., "Toroidally-wound self-bearing BLDC motor with lorentz force," IEEE Trans. Magn, Vol. 46-6, pp.2148-2151, 2010.

[6] Zu¨rcher F., Nussbaumer T., Kolar J. W., "Motor torque and magnetic suspension force generation in bearingless brushless multipole motors," IEEE/ASME Tran. Mech, Vol. 17-6, pp.1088-1097, 2012.

[7] Chiba A., Power D. T., "Rahman M. A.. Characteristics of a bearingless induction motor." IEEE Trans. Magn, Vol. 27-6, pp. 5199-5201, 1991.

[8] Rodriguez E. F., Santisteban J. A., "An improved control system for a split winding bearingless induction motor," IEEE Trans. Industrial Electronics, Vol. 58-8, pp. 3401-3408, 2011.

[9] Y.Okada,N.Yamashiro,K.Ohmori, T. Masuzawa, T.Yamane,Y.Konishi, and S. Ueno, "Mixed flow artificial heart pump with axial self-bearing motor," IEEE Trans. Mechatronics, vol. 10, no. 6, pp. 658–665, Dec. 2005.

[10] M.D.Noh, C. Seong-Rak, K. Jin-Ho, R. Seung-Kook, and P. Jong-Kweon, "Design and implementation of a fault-tolerant magnetic bearing system for turbo-molecular vacuum pump," IEEE Trans. Mechatronics, vol. 10, no. 6, pp. 626–631, Dec. 2005.

[11] A. Chiba, T. Fukao, O.Ichikawa, M. Oshima, M. Takemoto, and D. G. Dorrell, Magnetic Bearing and Bearingless Drives, NewYork: Elsevier, 2005.

[12] F. Z¨uricher, T. Nussbaumer, W. Gruber, and J. W. Kolar, "Comparison of 2- and 3-phase bearingless slice motor concepts," presented at the 11th Int. Symp. Magn. Bearings, Nara, Japan, 2008.

[13] S. Silber, W. Amrhein, P. Bosch, R. Schob, and N. Barletta, "Design aspects of bearingless slice motors," IEEE Trans. Mechatronics, vol. 10, no. 6, pp. 611–617, Dec. 2005.

[14] H. Grabner, H. Bremer, W. Amrhein, and S. Silber, "Radial vibration analysis of bearingless slice motors," presented at the 9th Int. Symp. Magn. Bearings, Lexington, KY, 2004.